# Supplementary Methods

## Preparation of yeast proteins

Endogenous *S. cerevisiae* ten-subunit Pol II core enzyme was prepared as described[1]. An *E. coli* expression vector was derived from pET21b (Novagen) for the co-expression of the translational fusion of *S. cerevisiae* Rpb4:20 glycine linker:TFIIB and Rpb7:$His_6$ under the control of separate T7 promoters. Details of the vector design are available on request. Following expression in *E. coli*, cells were lysed by sonication in buffer A (50 mM Tris, 150 mM NaCl; pH 7.5, 0.3 mg/L leupeptin, 1.4 mg/L pepstatin A, 0.17 g/L PMSF, 0.33 g/L benzamidine and 10 mM β -mercaptoethanol). The lysate was cleared by centrifugation and applied to a Ni-NTA agarose column (Qiagen). The column was washed with buffer A containing 2 M NaCl, and the protein was eluted with a gradient of 10 mM to 200 mM imidazole in buffer A containing 150 mM NaCl. Peak fractions were diluted twofold and loaded onto a Mono-S cation exchange column (Amersham) equilibrated with buffer A containing 100 mM NaCl. The fusion protein was eluted over a total of 15 column volumes with a gradient of 0.1–1 M NaCl in buffer A. Peak fractions were concentrated and applied to a Superose 6 gel filtration column (Amersham) equilibrated with buffer B (5 mM HEPES pH 7.25, 40 mM ammonium sulfate, 10 μM $ZnCl_2$, 10 mM DTT). Peak fractions were concentrated, shock-frozen in liquid nitrogen, and stored at –80°C. The TBP core domain (*S. cerevisiae* residues 61–240) expression vector was a generous gift from Dr. Sean Juo. Expression and purification of the yeast TBP core domain was as described[2] except that Superose 12 size exclusion chromatography was performed with buffer B. Peak fractions were concentrated, shock-frozen in liquid nitrogen, and stored at –80°C. 10-subunit Pol II was incubated with two molar equivalents of nucleic acid scaffold (Template, 5'-cgacacagcatcaaatgcacgatgtaacttttataggcgcccaacc; Nontemplate, 5'-ggttgggcgcctataaaagttacatcgtgcaaaatcgttatgagaa; RNA, 5'-gctgtgtcg) as described[3] and 2.5 molar equivalents of TBP. After incubation for 20 minutes at 20°C 3-5 molar equivalents of TFIIB-Rpb4/7 fusion protein were added. After incubation for 20 min. at 20°C, the complex was purified on a Superose 6 size exclusion column (Amersham). Fractions corresponding to the complex were pooled and concentrated to 4 mg/ml.

## Crystallization, data collection, and structure determination

Crystals were grown at 20 °C using the hanging drop vapor diffusion method by mixing 1.5 μl of sample solution with 1.5 μl of reservoir solution (800 mM sodium ammonium tartrate, 100 mM HEPES pH 7.5, 5 mM DTT). Crystals were transferred stepwise to mother solution containing additionally 0–22% glycerol over 8 h, slowly cooled down to 8 °C, incubated for another 24 h, and plunged into liquid nitrogen. Diffraction data were collected in 0.75° increments at the protein crystallography beamline ID 29 at ESRF. Diffraction data were processed with XDS and scaled with XSCALE[4]. The structure was solved by molecular replacement with PHASER[5] using the first 12-subunit Pol II without nucleic acids of the "EC I" complex[6]. The structure was refined with PHENIX[7] and with BUSTER[8] using TLS, group B-factors per residue, tight Engh-Huber geometrical restraints, and additional hydrogen-bond distance restraints for secondary structural elements (DK, unpublished data) against the observed data that were sharpened[9] with a B-factor of -80 $Å^2$. BUSTER was used

initially either with a coarse mask encompassing the whole Pol II cleft describing the expected region for the missing TFIIB (B) atoms, or by specifying the expected number of missing B atoms. In later refinement stages, no expectation of missing atoms was given. BUSTER produced clearer electron density maps, lower R-factor and Free-R-factor with better geometry. Data processing and refinement statistics are shown Supplementary Table 1.

*Supplementary Table 1*
X-ray diffraction data and refinement statistics

| | |
|---|---|
| *Data collection*[a] | |
| Space group | $C222_1$ |
| Unit cell axes [Å] | 221.0, 408.3, 275.2 |
| Wavelength [Å] | 0.9340 |
| Resolution [Å] | 40–4.3 (4.4–4.3)[b] |
| Completeness [%] | 99.3 (98.2) |
| Unique reflections | 83,919 (6050) |
| Redundancy | 4.7 (4.7) |
| $R_{sym}$ [%] | 13.2 (99.0) |
| $\langle I/\sigma I \rangle$ | 11.5 (2.0) |
| *Refinement* | |
| Amino acid residues | 4115 |
| Nonhydrogen atoms | 32,333 |
| RMSD bonds [Å] | 0.009 |
| RMSD angles [°] | 1.2 |
| $R_{cryst}$ [%][d] | 22.0 |
| $R_{free}$ [%][d] | 25.5 |
| 8 Zn peaks for Pol II in anomalous Fourier [σ][c] | 8.2, 9.2, 8.5, 8.4, 8.7, 5.4, 8.0, 7.6 |
| Zn peak for B in anomalous Fourier [σ][c] | 8.1 |

[a]Diffraction data were collected at beamline ID29 at the ESRF, Grenoble, France.
[b]Numbers in parenthesis refer to the highest resolution shell.
[c]Calculated at 6 Å resolution using phases from Pol II alone after initial refinement against observed data with separate Friedel pairs and without B-factor sharpening.
[d]Refinement was done against observed data with Friedel pairs merged and with an applied B-factor sharpening of -80 $Å^2$

**Electron density map interpretation**
Difference electron density omit maps after the first round of refinement of Pol II in the absence of B clearly showed the B-ribbon, the B-reader helix, B-linker strand, and the B-linker helix of B and the Pol II Rpb2 flap loop that got ordered upon B binding, and more weakly also the first B cyclin domain (N-terminal cyclin fold of B-core). An anomalous difference electron density map at 6 Å resolution clearly showed the position of the additional zinc belonging to the B-ribbon domain with a peak height of 8.1*σ over mean (Supplementary Figures 1, 2).

Using the zinc peak in the anomalous difference electron density map as a pivot point, the NMR structure of the zinc ribbon domain from *P. furiosus* TFB[10] was placed into the difference electron density map for the B-ribbon and used as a structural template to build the *S. cerevisiae* amino acid sequence including side chains that were partly visible. Model building was done with MOLOC using local real-space-refinement with energy optimization[11], resulting in stereochemically excellent models despite the

low resolution of the electron density maps. The cysteine residues involved in zinc binding helped to assign the amino acid sequence to the electron density maps. The density following the C-terminal end of the B-ribbon was too thick to accommodate a β-strand, resulting in positive difference electron density around it when a strand was included in refinement. Best refinement results with minimum residual difference densities were obtained by interpreting this electron density with a short α-helix from residues 59-68 (B-reader helix), with a large side chain electron density assigned to W63.

The B-core N-terminal cyclin fold showed weak electron density, which however allowed fitting of the known human domain structure[12]. There was only one possible orientation of the cyclin fold that explained the unbiased difference density peaks for the helices of the domain. To exclude model bias, two different models were refined, one with the cyclin fold in the correct orientation, and the other with the cyclin fold in an intentionally wrong orientation, perpendicular to the assumed correct orientation. For the correctly oriented domain, the electron density maps improved after refinement, but for the incorrectly oriented domain only those parts of the electron density improved where the incorrectly oriented α-helices crossed the electron density of the correctly oriented ones, and negative difference electron density appeared for the rest of the incorrectly placed cyclin domain. Thus, the correct and wrong orientation of the N-terminal cyclin domain could be clearly distinguished in the electron density maps despite the weak density. The close homology between human and yeast B-core domains allowed us to assign the corresponding yeast residue numbers to the fitted human domain, but we only modeled this domain as poly-alanine since side chains were not revealed. Consistent with this fit, salt bridges may be formed between B-core residues D138, K144, D147 and Rpb2 residues K451, D959, and K865, respectively. An alternative explanation of the densities with the related C-terminal cyclin fold was excluded because this resulted in a clash of the N-terminal cyclin fold with the Pol II protrusion (Supplementary Figure 3).

The B region connecting the B-ribbon and B-core domains was also iteratively built as poly-alanine using a tentative sequence number assignment according to *S. cerevisiae* B and secondary structure prediction. The resulting electron density was very convincing (Supplementary figure 4). The B-linker helix contained the only residues in the connecting region predicted to be helical (105-115), and connected to the N-terminal residue in the B-core, further arguing that the B-core density really results from the N-terminal cyclin fold of the B-core. The B-linker strand forms a short anti-parallel sheet with a strand in the rudder and contained residues predicted to be in a strand conformation. Extensive attempts to introduce selenomethionine labels in the connecting region failed due to low reproducibility of the crystals and diffraction. Since the B-linker strand is flanked by disordered loops on both sides and we do not have the resolution to reveal small side chains, it remains in principle possible that the B-linker strand is slightly out of register. Concerning the covalent linker between Rpb4/7 and B, several lines of evidence show that this linker does not give rise to artifacts in the positioning of B. First, the linker is more than twice the distance of the linked termini. Second, the linker is disordered in the density. Third, the linked B-ribbon is in the same position as previously observed in the absence of the linker. Forth, the linked B allowed for formation of a complex with TBP and nucleic acids, as described in supplemental, showing that it is functional in TBP and nucleic acid binding. The following two figures show the final and omit density maps.

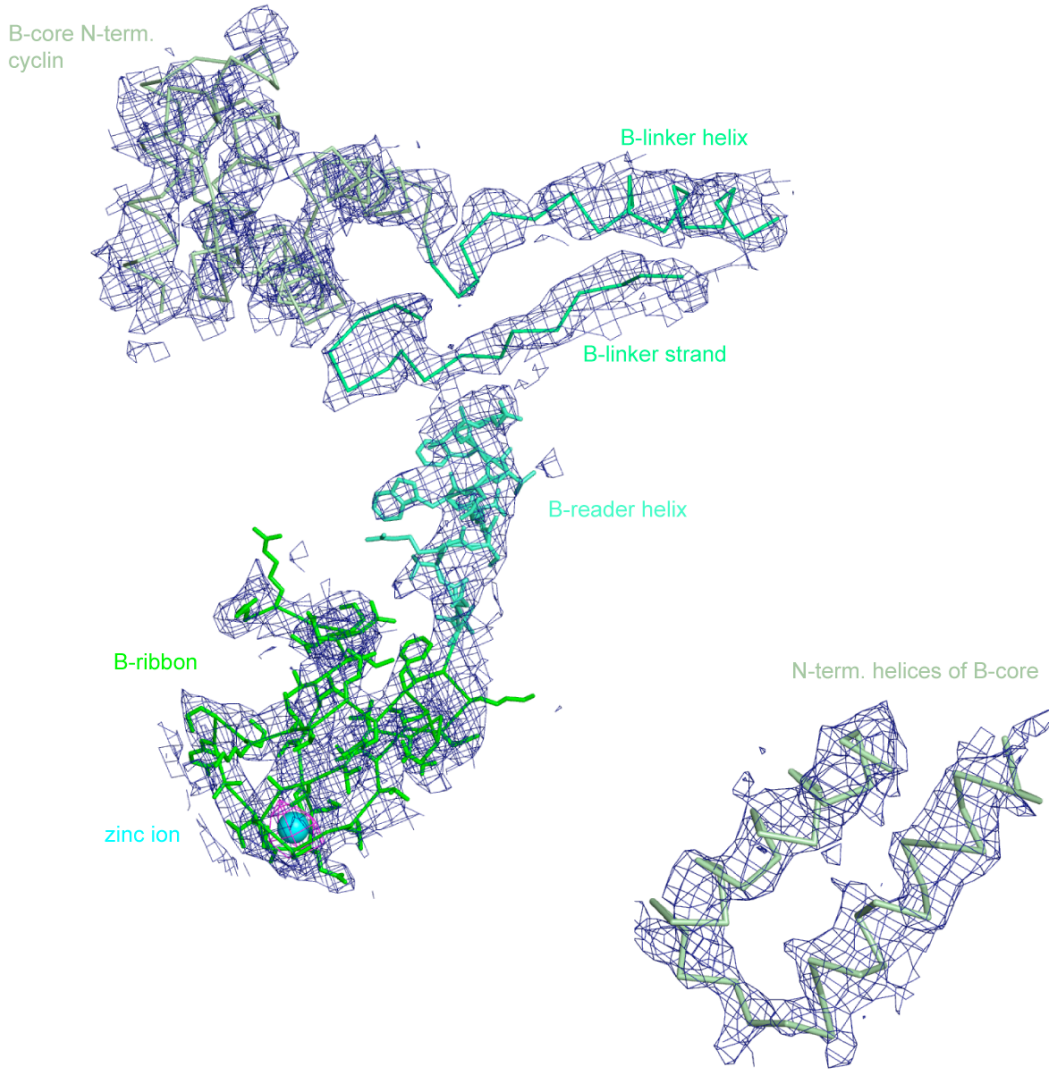


*Supplementary Figure 1*

Refined BUSTER 2mFo-DFc electron density maps (blue mesh), contoured at 1.0*σ for B-ribbon (green) and B-reader (cyan), and contoured at 0.8*σ for B-linker (turquoise) and B-core (pale green). The final structure of B is shown as a Cα trace with side chains for the B-ribbon and B-reader helix, and as a Cα trace for the remainder of the structure. The N-terminal helices of the B-core are shown as a close-up in the lower right corner. An anomalous difference Fourier peak is shown in magenta (5.0*σ) and indicates the location of the zinc ion in the B-ribbon. For clarity, maps are only shown within a radius of 3 Å around atoms.

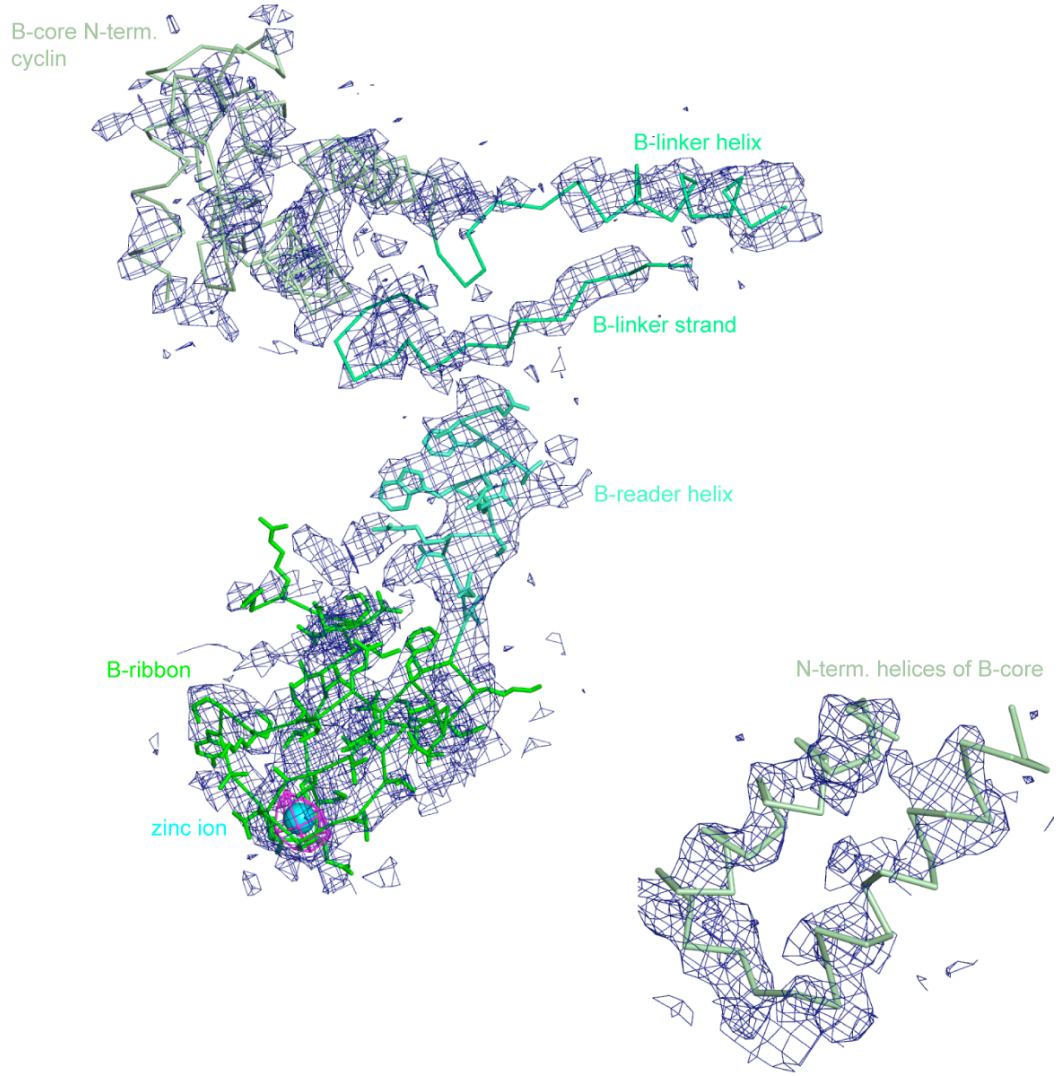


*Supplementary Figure 2*

Unbiased omit mFo-DFc difference electron density maps, contoured at 2.0*σ (blue mesh), were calculated with BUSTER after the first round of refinement with the Pol II structure alone. The final structure of B is shown as a Cα trace with side chains for the B-ribbon and B-reader helix, and as a Cα trace for the remainder of the structure. The N-terminal helices of the B-core are shown as a close-up in the lower right corner. An anomalous difference Fourier peak is shown in magenta (5.0*σ) and indicates the location of the zinc ion in the B-ribbon. For clarity, electron density maps are only shown within a radius of 5 Å around atoms. Note that even the highly mobile B-core cyclin fold domain shows clear density as demonstrated for the two N-terminal helices.

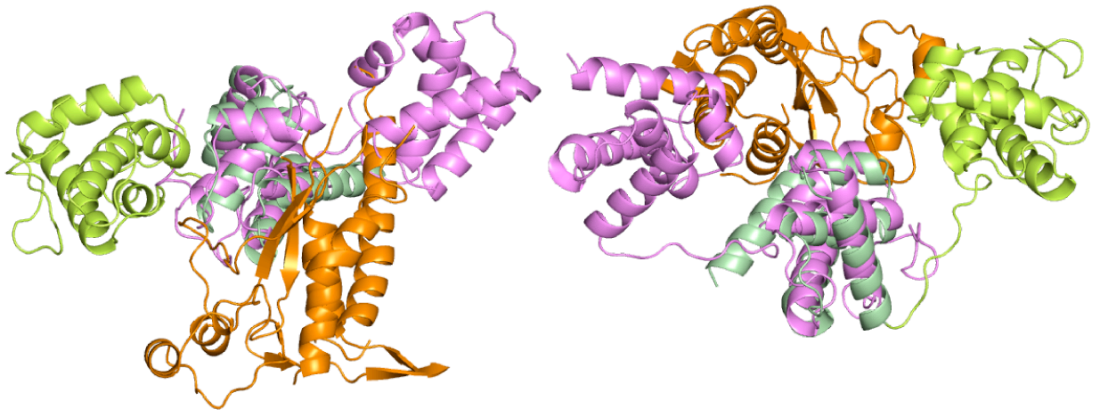

*Supplementary Figure 3*

**An alternative interpretation of the observed density for the B-core on the wall with the C-terminal cyclin fold is excluded since this would lead to a clash of the N-terminal cyclin fold with the Pol II protrusion domain.** Superposition of the structure of the two B-core cyclin domains based on the crystal structure of the N-terminal cyclin domain (N-terminal cyclin, pale-green; C-terminal cyclin, yellow-green), with the alternative location of the B-core cyclin domains (violet) if the electron density would have been interpreted with the C-terminal cyclin domain instead of the N-terminal cyclin domain. In the resulting position, the N-terminal domain would clash with the Pol II protrusion (orange). The left panel shows the side view, the right panel the top view (same side and top views as in main paper).

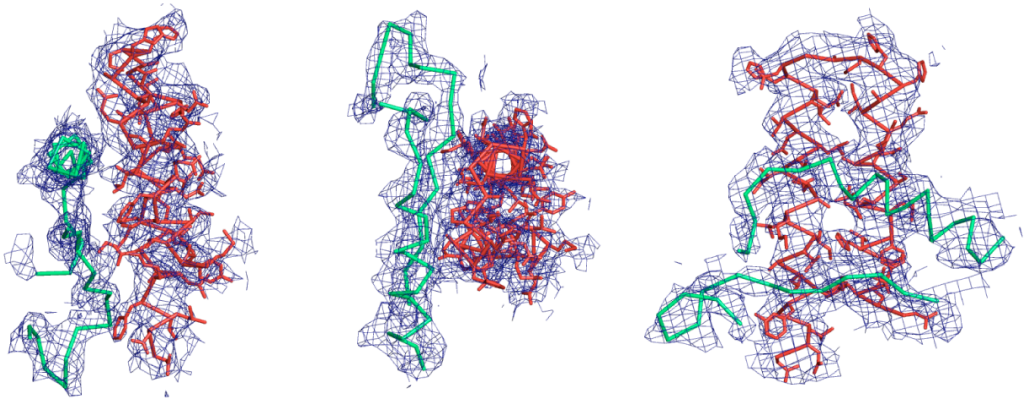

*Supplementary Figure 4*

**Final electron density for the B-linker and Pol II clamp coiled-coil.** The refined BUSTER 2mFo-DFc electron density map, contoured at 0.8*σ (blue mesh), is shown in three different orientations around the B-linker (turquoise Cα trace) and the neighboring Pol II clamp coiled-coil (red Cα trace with side chains as sticks). For clarity, electron density maps are only shown within a radius of 3 Å around atoms.

**The Pol II-B structure is consistent with biochemical probing of B within the PIC**
Hydroxyl radical cleavage probe sites[13] on the B-core that induce cleavage in the wall (I145, E184, D228), protrusion (Q127, M135, I145), and clamp (M135, I145) are adjacent in our structure. The location of the B-reader and B-linker is also consistent with hydroxyl radical-forming probe sites introduced into B and resulting in cleavage in the Pol II clamp (Supplementary Figure 5).

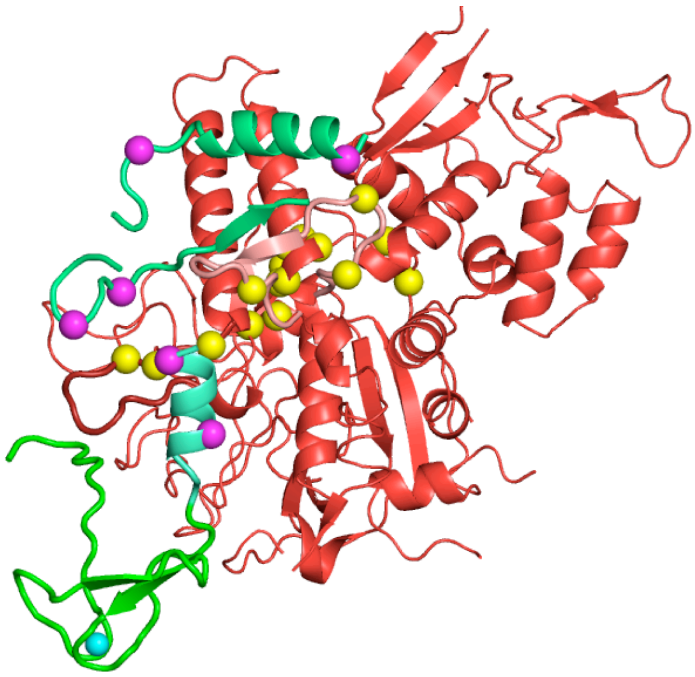

*Supplementary Figure 5*
Point mutations introducing hydroxyl radical-generating probe sites in the B-reader (cyan) and B-linker (turquoise) are indicated with magenta spheres[SN6]. The resulting radical cleavage sites in the Pol II clamp (red) are indicated with yellow spheres, and are consistent with our crystal structure of regions.

**Modeling the closed and open complexes**
Models were built with MOLOC using energy optimization for TBP, the C-terminal cyclin fold of B, and DNA, while keeping the crystal structures of Pol II in complex with B and the superimposed active site DNA of the complete Pol II elongation complex fixed, except for removing a few local steric clashes.

**Calculation of omit electron density maps for the 10-subunit core Pol II-B complex using published data from Bushnell et al.[14]**
The coordinate file in PDB format of the previously published 10-subunit Pol II structure in complex with B, 1R5U.pdb, was downloaded together with the corresponding observed structure factor amplitudes, 1R5U-sf.cif, from the Protein Data Bank. The reported refinement statistics were: R=34.5%/$R_{free}$=37.3% for 57395 reflections between 50–4.5 Å resolution. For all subsequent calculations, chain M with coordinates of B and its bound zinc ion, M209, were omitted from the coordinate file 1R5U.pdb to reduce any potential model bias coming from B. The resulting coordinate file is named 1R5U-omit.pdb. The observed structure factor amplitudes were converted from the MMCIF format into the CCP4 MTZ format with the program CIF2MTZ after re-mapping and re-ordering of corresponding Friedel pairs

(DK, personal communication). The program MTZ2VARIOUS was used to convert the MTZ format into X-PLOR format. The data set with unmerged Friedel pairs was used for calculating anomalous difference electron density maps. The data set with merged Friedel pairs was used for refinement and for calculation of omit maps. In total, 111,201 reflections were read from the original MMCIF file, of which were 53,456 Friedel pairs, 5 acentric reflections without a Friedel mate and 4284 centric reflections. Care was taken that reflections belonging to the test set in the original MMCIF file, which were marked with "f", were correctly marked with "0" in the MTZ file, and with "1" in the X-PLOR file.

The software suite CNS 1.2[15,16] was used to calculate initial model statistics with mask bulk solvent correction for 1R5U-omit.pdb. CNS reproduced the published anisotropic scaling factors within a few percent, and reported an R-factor of 31.8% and a Free-R-factor of 34.8%, both of which were ≈3% lower than the reported values for 1R5U.pdb. Using the model phases of 1R5U-omit.pdb, an anomalous difference electron density map was calculated at a maximum resolution of 6 Å. The anomalous difference electron density map, contoured at a level of 6*σ, showed strong positive peaks around the positions of six of the eight zinc ions bound to Pol II, and it showed a peak around the position of the omitted zinc ion M209 bound to the B-ribbon. The similarity of the scaling factors and the R-factors reported by CNS, and the clear peak in the anomalous difference electron density map around the omitted zinc atom M209 indicated that the deposited observed structure factor file 1R5U-sf.cif indeed belongs to the deposited coordinate file 1R5U.pdb used by Bushnell et al. in the structure solution and refinement of the 10-subunit Pol II-B complex.

Initial omit maps calculated with CNS 1.2 with mask bulk solvent correction showed clear 2mFo-DFc-density, contoured at 1*σ, and mFo-DFc-density, contoured at 3*σ, for large parts of the B-ribbon until residue M57. After this position, the electron density became significantly thicker. However, for the previously modeled B-finger domain from M61 until M88 there was no electron density for the trace deep into the active center of Pol II, except for residues M85 and M86 that were traced back through the thicker electron density opposite to M59 and M60. Contouring the omit electron density maps at lower levels increased the noise of these maps, but did not reveal electron density for the B-finger. The CNS omit map from 1R5U-omit.pdb is more consistent with our B-reader structure than with the B-finger structure of Bushnell et al. (Supplementary Figure 6).

To exclude any potential reduction of the local contrast by the mask bulk solvent correction used in CNS, we repeated the calculation of the omit electron density maps without any bulk solvent correction. This led to an increased R-factor of 39.4% and a Free-R-factor of 42.2%. The resulting omit electron density maps still showed no electron density for a B-finger. To further explore the absence of the B-finger, we re-refined 1R5U-omit.pdb against the observed structure factors with state-of-the-art crystallographic refinement programs REFMAC5 and PHENIX, and calculated the corresponding electron density maps. In REFMAC5, we calculated 10 cycles of TLS refinement using one TLS group for the whole structure, followed by 30 cycles restrained maximum-likelihood positional and B-factor refinement using the mask bulk solvent correction. A control refinement using the Babinet bulk solvent correction was done to exclude any potential lowering of the local contrast by the mask bulk solvent correction. This refinement had to be stopped after 26 cycles

maximum-likelihood refinement because it became unstable. The final R-factors were R=27.3%/$R_{free}$=30.5% using the mask bulk solvent correction, and R=32.7%/$R_{free}$=37.5% using the Babinet bulk solvent correction, respectively. The final RMSD of bond lengths was 0.011 Å for both refinements. Despite the lower R-factors in case of the refinement using the mask bulk solvent correction, the resulting omit electron density maps did not show electron density for a B-finger. The refinement using the Babinet bulk solvent correction showed a slightly lower R-factor and a similar free-R-factor as reported for 1R5U. Again, the resulting omit electron density maps did not show electron density for a B-finger. With PHENIX, we carried out 3x25 cycles of TLS refinement using one TLS group for the whole structure, together with a mask bulk solvent correction and restrained maximum-likelihood positional and group B-factor refinement for each residue. The final R-factors were R=22.9%/$R_{free}$=28.3% with an RMSD of bond lengths of 0.010 Å. The final free R-factor was about 9% lower than that published. Nevertheless, no electron density for a B-finger was observed.

To summarize, we could reproduce the anomalous signal of the zinc atom bound to B and the omit electron density map showing the B-ribbon. However, with none of the state-of-the-art refinement programs, we could detect significant electron density for a B-finger, despite obtaining much lower R-factors and Free-R-factors and very good stereochemistry for the models. It is generally accepted that a lower Free-R-factor correlates well with lower phase errors. To the best of our efforts, we could not reproduce the evidence reported by Bushnell et al. for a B-finger structure in B. Instead, all densities we obtained with the deposited structure factors were consistent with the B-reader helix observed by us.

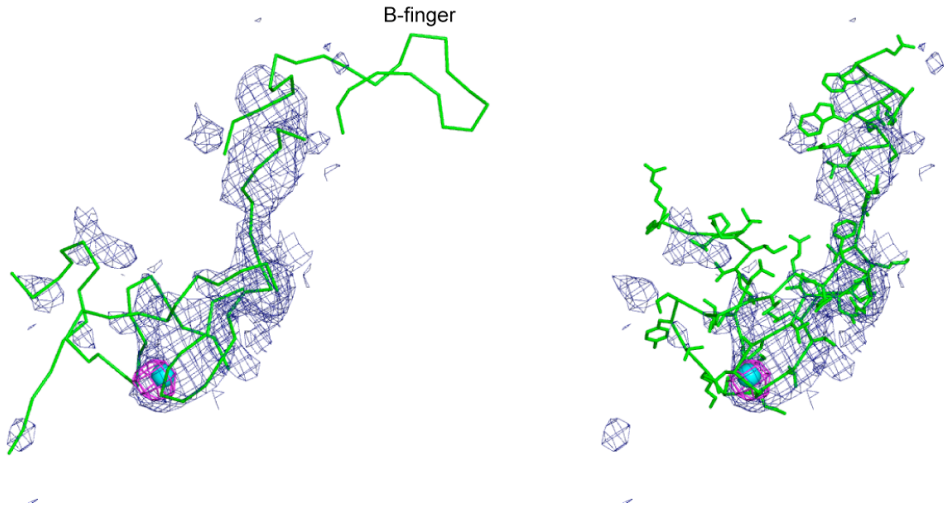


*Supplementary Figure 6*
Unbiased CNS omit mFo-DFc electron density, contoured at 2*σ (blue mesh), for the structure of Bushnell et al., shown with the B structure of Bushnell et al. (left, green Cα trace) and with our B-ribbon superimposed on the B-ribbon of Bushnell et al. (right, green Cα trace with side chain sticks). Please, note the missing density for the B-finger. An anomalous difference Fourier peak is shown in magenta (5.0*σ) and indicates the location of the zinc ion in the B-ribbon. For clarity, electron density maps are only shown within a radius of 5 Å around atoms.

***P. furiosus* protein preparations**

Endogenous *P. furiosus* (*Pfu*) RNA polymerase and recombinant *Pfu* TBP were purified as described[17]. *Pfu* TFB was cloned with an N-terminal $His_6$-Tag in pET14b (Novagen) in *E. coli* BL21(DE3)pLysS (Novagen). Cells were grown in LB medium in the presence of ampicillin (100 mg/l) and chloramphenicol (50 mg/l) until $OD_{600}$ = 0.8 was reached, transferred to ice for 30 min, and followed by induction at 0.5 mM IPTG for 18 hours at 18°C. After one freeze/thaw cycle, cell pellets were resuspended in binding buffer (50 mM $NaH_2PO_4$ pH 8.0, 300 mM NaCl, 10 mM imidazole, 10% glycerol, 5 mM 2-mercaptoethanol, 0.5 mM PMSF). Cells were disrupted using three passes through a French press. After centrifugation for 30 min at 20,000 rpm (JA-10 rotor), *E. coli* proteins in the supernatant were partly removed by heat treatment for 15 min at 70°C and centrifugation for 20 min at 20,000 rpm (JA-25.50 rotor). The supernatant was applied to a Ni-NTA column (5 ml HisTrap Chelating HP, GE Healthcare). TFB eluted at 200 mM imidazole within a linear gradient of 10 column volumes up to 500 mM imidazole. A co-eluting N-terminal fragment was removed by gel filtration using a HiLoad 16/60 Superdex 75 column (GE Healthcare) preequilibrated with 20 mM HEPES-Na pH 7.8, 250 mM NaCl, 0.5 mM EDTA, 10% glycerol, 5 mM 2-mercaptoethanol, 0.5 mM PMSF. TFB concentrations were measured by the method of Bradford and further adjusted by Coomassie blue staining after SDS PAGE. RNAP subunits were purified as described[18], with 2 exceptions. *i)* A' was obtained by stepwise elution rather than gradient elution from a Ni-NTA column (5 ml HisTrap Chelating, GE Healthcare). Briefly, after on-column refolding, the column was washed with 10 column volumes refolding buffer (20 mM Tris-HCl pH 8, 500 mM NaCl, 20 mM imidazole, 5 mM 2-mercaptoethanol, 0.5 mM PMSF) and 4 column volumes 40 mM imidazole. A' was eluted at 200 mM imidazole. *ii)* A'' was purified from supernatants obtained from inclusion body washes with IB buffer (20 mM Tris-HCl pH 8, 2 M urea, 500 mM NaCl, 0.1% Tween, 5 mM 2-mercaptoethanol, 0.5 mM PMSF), as most of A'' protein was soluble therein. Supernatants were applied to a Ni-NTA column (5 ml HisTrap Chelating HP, GE Healthcare); urea was removed by a linear gradient of 10 column volumes to IB buffer without urea. After washing with additional 10 column volumes, A'' was eluted within a linear gradient of 15 column volumes up to 500 mM imidazole. Reconstitution of recombinant RNAPs was performed as described[18]. Concentrations of mutant RNAPs were estimated by comparison with a standard RNAP of known concentration on Sypro Orange (Invitrogen) stained SDS polyacrylamid gels.

***P. furiosus* transcription assays**

Standard transcription template *gdh-C20*[19] was generated by PCR using M13 primers, following purification with the Qiagen PCR purification kit. The 297 bp PCR product contains the promoter region of a modified version of the *Pfu gdh*-gene, where the first cytidine in the RNA-coding strand occurs at position +20. Run-off transcription yields a 113 nt RNA product. Open templates contained mismatches at position -9, -10 and -11 ("*open upstream*") or -2, -1 and +1 ("*open start*") relative to the transcription start site in *gdh-C20* and were prepared as reported[20]. Briefly, mutations were introduced by fusion PCR. Mutant and original DNA sequences were PCR amplified using one phosphorylated and one unphosphorylated primer. The phosphorylated strand was specifically digested with λ-exonuclease (Fermentas). Wild-type template strand and mutant nontemplate strand were mixed in equimolar amounts, re-annealed in 10 mM Tris-HCl pH 8 (5 min 95°C, 15 min 45°C, 15 min 40°C) and purified from agarose gels using the Qiagen gel extraction kit. For direct

comparison, "*closed*" templates were prepared in the same way, except that both template and nontemplate strand were derived from wild-type sequence. Synthetic oligonucleotide templates were generated as described[21]. Run off transcription was carried out as described[18]. Briefly, 10 nM *gdh-C20* template, 200 nM TBP, 70 nM TFB and 10 nM RNAP in a final volume of 25 $\mu$l were incubated in transcription buffer containing NTPs (440 $\mu$M ATP, 440 $\mu$M GTP, 440 $\mu$M CTP, 2.7 $\mu$M UTP and [$\alpha$-$^{32}$P]UTP at 0.15 MBq (110 tBq/mmol) for 15 min at 70°C. Transcription with "*closed*", "*open upstream*" and "*open start*" templates contained 15 nM template. Abortive transcription was carried out with the indicated template, 40 $\mu$M GpU (Sigma), [$\alpha$-$^{32}$P] UTP at 0.22 MBq (110 tBq/mmol), but without radioactive NTPs. Experiments using DNA templates formed from synthetic oligonucleotides were previously established[22]. RNA was extracted with phenol-chloroform and analyzed by electrophoresis in a 8% (run-off) or 28% (trinucleotides and short transcripts) polyacrylamide/urea gel.

**Other *P. furiosus* biochemical assays**

Bandshift assays with reconstituted RNAPs were performed as described[22]. Experiments with mutant TFBs were carried out using a fluorescent *gdh-C20* template that was generated by PCR with a Cy5-labeled M13-reverse primer. Binding reactions were performed in transcription buffer (40 mM HEPES-Na pH 7.3, 250 mM NaCl, 2.5 mM $MgCl_2$, 5% glycerol, 0.1 mg/ml BSA, 1 mM DTT, 0.1mM EDTA) and containted 100 nM template, 200 nM TBP, 70 nM TFB and 20 nM endogenous RNAP in a final volume of 25 $\mu$l. After 10 min pre-incubation at 70°C, the reaction was cooled to 4°C, 1 $\mu$g of poly(dI-dC) (Fluka) was added as competitor DNA, and incubation at 70°C was continued for 15 min. 17 $\mu$l of the reaction were loaded on a 4.5% polyacrylamide/2% glycerol/TBE gel. Results were visualized on a Fuji FLA-5000 Phosphoimager. Potassium permanganate footprints were performed on immobilized templates as previously established[21]. Initiation complexes were formed with 200 nM TBP, 70 nM TFB and 75 nM RNAP.

**Yeast strains and *in vitro* assays**

The heterozygous strain *SUA7/sua7D* gene (Open Biosystems) was transformed with centromeric plasmid pRS316_TFIIB[23], containing 500 bp upstream and 300 bp downstream of the *SUA7* open reading frame and a *URA3* marker. Diploids were sporulated and tetrads were dissected on YPD plates. The *SUA7* shuffle strain was transformed with pRS315_TFIIB[23], containing either wild type or mutant B variants. Effects of mutations in B were assessed by selection on 5-FOA medium. Viable strains were re-stroked on FOA-medium and YPD. Growth of strains was assessed at 16°C, 28°C and 30°C with spot dilutions on YPD plates and by recording growth curves in YPD medium. All growth experiments were performed in triplicate. Nuclear extracts were prepared from wild-type and strain SHY245[24] as described by the Hahn laboratory (www.fhcrc.org/labs/hahn). *In vitro* transcription was performed as reported[24,25], except that 5 nM Cy5-labelled primer (5'-ttcaccagtgagacgggcaac) were used for primer extension and a plasmid containing the *HIS4-SNR14* (pMSe24) or the indicated promoter was used as template. Template plasmids were obtained by mutagenesis of pSH515[24], containing a modified *HIS4* core promoter and a single Gal4 binding site. Start sites were determined using dideoxy sequence ladders generated with the same primer (Sequencing Kit, USB). RNA products were separated on 8% polyacrylamide/ urea gels and visualized on a Typoon 400 scanner (GE Healthcare).

**Preparation of recombinant yeast TFIIB variants**

B was cloned with a C-terminal $His_6$-tag, expressed in *E. coli* BL21(DE3)CodonPlus (Novagen) in the presence of ampicillin (100 mg/l) and chloramphenicol (50 mg/l) until $OD_{600}$ = 0.8-1 was reached. The culture was transferred to ice for 30 min, followed by induction at 0.5 mM IPTG for 18 hours at 18°C. Cells were harvested by centrifugation at 6,000 rpm (SLC-6000 rotor) for 10 min at 4°C, resuspended in freezing buffer (50 mM Tris-HCl pH 7.5, 150 mM NaCl, 5% glycerol) and frozen in liquid nitrogen. Cells were thawed and disrupted by sonication for 15 min. The lysate was centrifuged at 13,000 rpm (SS34 rotor) for 45 min at 4°C, the supernatant was adjusted to 500 mM NaCl and applied to Ni-NTA beads (Qiagen) pre-equilibrated with binding buffer (50 mM Tris-HCl pH 7.5, 500 mM NaCl). After incubation on a rotary shaker for 1 hour at 4°C, beads were washed twice with binding buffer containing 5 mM imidazole. B was eluted with 250 mM imidazole. The sample was adjusted to 150 mM NaCl, concentrated by ultracentrifugation (Amicon, Millipore, MWCO 10,000 Da) and applied to a MonoS 5/5 column (GE Healthcare). B was eluted during a linear gradient of 15 column volumes to 575 mM NaCl. A contaminating C-terminal fragment was largely removed by an additional gel filtration step, using a Superose 6 column (GE Healthcare) that was equilibrated to 5 mM HEPES-Na pH 7.3, 40 mM ammonium sulfate, 5% glycerol, 10 $\mu$M $ZnCl_2$. B, TFB and RNAP subunit A' were mutated using the QuickChange II site-directed mutagenesis kit (Stratagene).

## Supplementary References


1. Armache, K.-J., Kettenberger, H. & Cramer, P. Architecture of the initiation-competent 12-subunit RNA polymerase II. *Proc. Natl. Ac. Sc. USA* **100**, 6964-6968 (2003).
2. Tan, S., Hunziker, Y., Sargent, D.F. & Richmond, T.J. Crystal structure of a yeast TFIIA/TBP/DNA complex. *Nature* **381**, 127-51 (1996).
3. Kettenberger, H., Armache, K.-J. & Cramer, P. Complete RNA polymerase II elongation complex structure and its interactions with NTP and TFIIS. *Mol. Cell* **16**, 955-965 (2004).
4. Kabsch, W. *J. Appl. Cryst.* **26**, 795-800 (1993).
5. McCoy, A.J. et al. Phaser crystallographic software. *J Appl Crystallogr* **40**, 658-674 (2007).
6. Sydow, J.F. et al. Structural basis of transcription: mismatch-specific fidelity mechanisms and paused RNA polymerase II with frayed RNA. *Mol Cell* **34**, 710-21 (2009).
7. Zwart, P.H. et al. Automated structure solution with the PHENIX suite. *Methods Mol Biol* **426**, 419-35 (2008).
8. Bricogne, G., Blanc, E., Brandl, M., Flensburg, C., Keller, P. et al. *"BUSTER-TNT, version 2.5.1"*, (United Kingdom: Global Phasing Ltd. , Cambridge, 2008).
9. DeLaBarre, B. & Brunger, A.T. Considerations for the refinement of low-resolution crystal structures. *Acta Crystallogr D Biol Crystallogr* **62**, 923-32 (2006).

10. Zhu, W. et al. The N-terminal domain of TFIIB from Pyrococcus furiosus forms a zinc ribbon [letter]. *Nat. Struct. Biol.* **3**, 122-124 (1996).
11. Gerber, P.R. & Muller, K. MAB, a generally applicable molecular force field for structure modelling in medicinal chemistry. *J Comput Aided Mol Des* **9**, 251-68 (1995).
12. Nikolov, D.B. et al. Crystal structure of a TFIIB-TBP-TATA-element ternary complex. *Nature* **377**, 119-128 (1995).
13. Chen, H.T. & Hahn, S. Mapping the location of TFIIB within the RNA polymerase II transcription preinitiation complex: a model for the structure of the PIC. *Cell* **119**, 169-80 (2004).
14. Bushnell, D.A., Westover, K.D., Davis, R.E. & Kornberg, R.D. Structural basis of transcription: an RNA polymerase II-TFIIB cocrystal at 4.5 Angstroms. *Science* **303**, 983-8 (2004).
15. Brunger, A.T. Version 1.2 of the Crystallography and NMR system. *Nat Protoc* **2**, 2728-33 (2007).
16. Brunger, A.T. et al. Crystallography & NMR system: A new software suite for macromolecular structure determination. *Acta Crystallogr D Biol Crystallogr* **54**, 905-21 (1998).
17. Hethke, C., Geerling, A.C., Hausner, W., de Vos, W.M. & Thomm, M. A cell-free transcription system for the hyperthermophilic archaeon Pyrococcus furiosus. *Nucleic Acids Res* **24**, 2369-76 (1996).
18. Naji, S., Grunberg, S. & Thomm, M. The RPB7 orthologue E' is required for transcriptional activity of a reconstituted archaeal core enzyme at low temperatures and stimulates open complex formation. *J Biol Chem* **282**, 11047-57 (2007).
19. Spitalny, P. & Thomm, M. Analysis of the open region and of DNA-protein contacts of archaeal RNA polymerase transcription complexes during transition from initiation to elongation. *J Biol Chem* **278**, 30497-505 (2003).
20. Thomas, E., Pingoud, A. & Friedhoff, P. An efficient method for the preparation of long heteroduplex DNA as substrate for mismatch repair by the Escherichia coli MutHLS system. *Biol Chem* **383**, 1459-62 (2002).
21. Naji, S., Bertero, M.G., Spitalny, P., Cramer, P. & Thomm, M. Structure-function analysis of the RNA polymerase cleft loops elucidates initial transcription, DNA unwinding and RNA displacement. ***36***, 676-87 (2008).
22. Reich, C. et al. The archaeal RNA polymerase subunit P and the eukaryotic polymerase subunit Rpb12 are interchangeable in vivo and in vitro. *Mol Microbiol* **71**, 989-1002 (2009).
23. Sikorski, R.S. & Hieter, P. A system of shuttle vectors and yeast host strains designed for efficient manipulation of DNA in Saccharomyces cerevisiae. *Genetics* **122**, 19-27 (1989).
24. Ranish, J.A., Yudkovsky, N. & Hahn, S. Intermediates in formation and activity of the RNA polymerase II preinitiation complex: holoenzyme recruitment and a postrecruitment role for the TATA box and TFIIB. *Genes Dev* **13**, 49-63 (1999).
25. Koschubs, T. et al. Identification, structure, and functional requirement of the Mediator submodule Med7N/31. *EMBO J* **28**, 69-80 (2009).